# Mechanical Characterisation of Pneumatically-Spliced Carbon Fibre Yarns as Reinforcements for Polymer Composites

# Mechanical Characterisation of Pneumatically-Spliced Carbon Fibre Yarns as Reinforcements for Polymer Composites

James R. Davidson, James A. Quinn, Claudia Rothmann, Ankur Bajpai, Colin Robert, Conchúr M. Ó Brádaigh, Edward D. McCarthy

*School of Engineering, Institute for Materials and Processes, The University of Edinburgh, UK*

*Postal Address: Sanderson Building, King's Buildings, Edinburgh, EH9 3FB, Scotland, UK*

**Abstract**

An investigation into the mechanical response of pneumatically-spliced carbon fibre yarns as a potential reinforcing material for polymer composites is presented. High strength mechanical connections between carbon fibre yarns are produced by joining short discontinuous tows into longer lengths via fibre entanglement. The effect of altering the number of high-pressure air pulses fired by a commercially available (Airbond 701H) splicing machine, to form the tow-tow connection, on load bearing capacity and linear stiffness is first evaluated on splices between virgin T700SC-24K-50C carbon fibre tows. The best performing spliced configuration is subsequently utilised in reinforcing unidirectional epoxy laminates, which are mechanically characterised, and their properties compared to those of various continuous fibre and chopped strand mat panels. Results presented in this study demonstrate that pneumatic splicing provides a high strength and sustainable solution for reinforcing polymers with discontinuous (approx. >50mm in length) virgin, off-cut or waste carbon fibre yarns. It is speculated that with further research, quasi-continuous yarns remanufactured by splicing waste fibres could provide a novel material for weaving, braiding, non-crimp fabrics, or use in 3D printing applications.

*Keywords:* Pneumatic Splicing, Carbon Fibres, Waste, Mechanical Testing

## 1. Introduction

Fibre reinforced plastic (FRP) materials exhibit exceptional specific strength, stiffness, and corrosion resistance properties. Popular reinforcing materials include glass fibres, which dominate the industry with a global demand volume (GDV) of 5.3M tonnes and carbon fibres with a GDV of 0.1M tonnes per annum [1]. Composite materials can actively help limit $CO_2$ emissions by reducing the weight of structural components, thereby lowering fuel consumption and emissions, as well as improving longevity in corrosive environments [2, 3]. This has driven composite adoption within sustainable engineering

*Email address:* J.R.Davidson@ed.ac.uk (James R. Davidson)

solutions but has indirectly led to other environmental repercussions. For instance, waste disposal and recycling concerns have been raised due to a lack of rapid and affordable end-of-life solutions [4]. An estimated 30-40% of composite materials are wasted during production, in the form of offcuts and trimmings [5]. Environmental and cost implications from material waste will increase in severity as rate of manufacture increases. [6].

A potential opportunity for remanufacturing virgin off-cut, waste or perhaps even recycled carbon and glass fibres may come through utilising pneumatic splicing techniques for joining discontinuous separate fibre-tows (of a few centimeters in length) [7], to form a reconstituted "quasi-continuous" yarn. These reconstituted tows have the potential to be utilised as reinforcing materials in unidirectional configurations (see subsequent sections), non-crimp fabrics, woven fabrics, 3D printing and in braiding processes, opening entirely new avenues for the manufacture of sustainable composite materials. Given that splicing technologies for high performance fibre reinforcements are to date almost unstudied in the published domain [8], this work aims to provide a foundation for understanding the basic mechanics of spliced carbon fibre tows, and their structural response when embedded within thermosetting polymers.

### *1.1. Background*

The pneumatic splicing methodology originates from the textile industry [7]; with recent technological developments and commercialisation facilitating implementation on larger, stiffer yarns. By overlapping two separate yarn ends, placing them together and agitating the fibres with turbulent air, a consistent and strong mechanical bond is created [9]. Conventionally, this involves passing high-speed air through a small hole and into a specially designed chamber containing the overlapped tows. As the blast enters the splicing chamber, the fibres within are split into two discrete bundles and rapidly moved upwards and outwards. Contra-rotating vortices subsequently twist the fibre bundles in opposing directions, throughout which, filaments intermingle and entangle. Intermingling occurs via filament migration- a process primarily investigated in the context of false-twist crimping [10]. In filament migration, spiralized bundles are produced with steep helix angles, leading exterior fibres to become highly stressed. These external fibres are continually forced inwards, whist inner fibres are pushed outwards, due to loading equilibrium requirements. Connections in which filaments spiral towards and away from the centre are eventually formed, where individual fibre stresses (exerted via friction and entanglement) are approximately equal throughout [11, 12]. The highly entangled and intermingled fibres produced from the pneumatic splicing method facilitate tensile forces to be transferred between yarns through fibre-fibre friction and interlocking mechanisms. The extent of entanglement varies continuously along the length of the fibre axis, with a single pulse from the splicer leading to discrete central, highly intermingled, and tail-end regions. A schematic diagram of the splicing process using an Airbond 701H hand-held splicer, which indicates these regions on an spliced connection discussed in

subsequent sections, is shown in Figure 1. Splice performance is material specific and heavily dependent on manufacturing specifications (for example, chamber design and filament size or quantity) [13]. To confront uncertainties associated with pneumatic splicing techniques, studies have been carried out relating to these splicing conditions for materials used in the textiles industry, alongside fluid-structure interaction models [14, 15, 16].

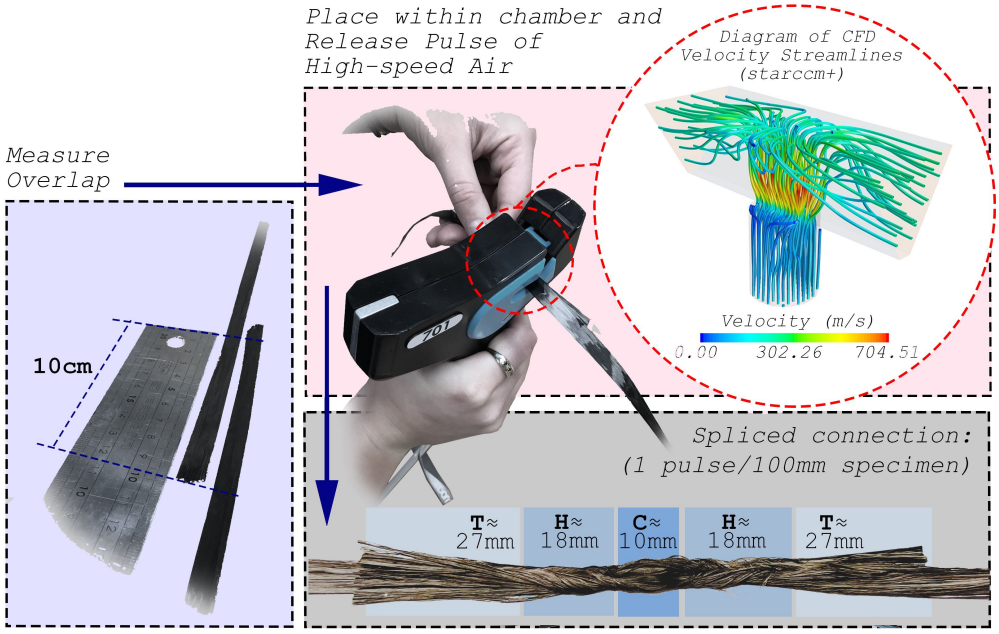


Figure 1: Schematic diagram for manufacturing pneumatically spliced (dry-fibre) specimens, where typical (1 pulse/100mm specimen) lengths are provided for the central (C), highly intermingled (H), and tail-end (T) regions.

### *1.2. Aims and Objectives*

The present work aims to assess the tensile performance of polymer composites reinforced with spliced carbon fibre tows. An initial investigation was first conducted on the performance of (non-embedded) dry-fibre specimens. Numerous parameters affect the dry-fibre connection strength and stiffness; these include: charge pressure, chamber design, yarn count and surface properties. In previous studies, optimisation methods have been used to overcome the extensive input data needed to produce numerical simulations. Notably, a Taguchi design of experiments (DOE) approach characterised the effect of key parameters for splicing nylon-66 yarn [14]. The innately random nature of the process also requires extensive data sets to accurately clarify trends and quantify variance. For these reasons, the charge pressure, overlap length, chamber design and yarn count were all kept constant in this work. Charge pressure, yarn count and chamber design parameters were chosen based on (Airbond Ltd)

manufacturer recommendations. An overlap length of 100mm was selected to ensure that tows could be easily handled, whilst also being sufficiently long to evaluate the effect of increasing the number of pulses (per unit length) on mechanical performance. Although evaluating this technique on longer overlaps is feasible, a relatively short overlap was considered in this preliminary investigation, since recycled or waste fibre tows are more readily available in shorter lengths. The quantity of fired pulses for a given overlap length, denoted specific pulse count (SPC, in pulses/100mm), was selected as the independent variable, since it was observed to have significant ramifications on mechanical performance of dry-fibre connections.

The optimum dry-fibre configuration, based on asymptotic regression trends for strength and linear stiffness, was then investigated as potential reinforcement in unidirectional panels. Asymptotic regression functions were defined for linear stiffness and strength, with respect to SPC. As before, a substantial number of design parameters strongly affect performance, with investigation scope being limited by the system complexity and numerous potential experimental variables. The manual fabrication and arranging of tows also limits the spectrum of design configurations. Due to the fibre count doubling at the overlap region, splices may cause unacceptable local rises in fibre volume fraction without careful consideration. By strategically staggering the position of the splices, this effect is minimised. Plates of staggered spliced-carbon fibre tows within an epoxy matrix were manufactured and tested. For comparison and general reference, unidirectional and chopped strand mat composite plates were manufactured based on an identical material system.

## 2. Experimental Procedure

### *2.1. Dry-fibre Specimens*

*Materials.* Splices were formed using Toray T700SC-24K-50C carbon fibre (density 1.80g/cm$^3$). Each tow contains 24,000 "never-twisted" filaments. A general purpose sizing with no surface treatment has been applied by the manufacturer, which accounts for 1% of the overall material volume (additional details are listed in Table 1) [17].

Table 1: Materials Data [18, 19]

| | | |
|---|---|---|
| T700SC-24K-50C (Carbon Fibres) | Density (g/cm$^3$) | 1.800 |
| | Tensile Strength (MPa) | 4900.0 |
| | Young's Modulus (GPa) | 230.0 |
| | Filament Diameter ($\mu$m) | 7.0 |
| | Tow Yield (g/cm) | 165.0 |
| PE6405 Epoxy Powder (after curing) | Density (g/cm$^3$) | 1.22 |
| | Tensile Strength (MPa) | 73.0 |
| | Young's Modulus (GPa) | 3.0 |

*Manufacture.* For specimen assembly, an Airbond 701H splicer was charged to 690kPa via mains high-pressure air. Per each sample, 2×600mm lengths of carbon-fibre tows were cut from a bobbin and longitudinally overlapped by 100mm. The overlapped region was subsequently positioned inside the splicing chamber. Upon triggering pressure discharge for 1.5 seconds, a pulse of turbulent air was released, locally entangling the filaments and forming a discrete spliced zone. Eight variations of dry-fibre spliced samples were manufactured, in which SPC was the independent variable. For each variation, the number of air pulses (discharged at equidistant points along the overlap) increased from 1 pulse (1 pulse/100mm) to 15 pulses (15 pulses/100mm) by a fixed interval of two units each time. For statistical accuracy, 75 specimens were tested for each SPC, based on observed probability density distributions. Sample firing sequences and discharge locations for all configurations are displayed in Figure 2(a). In measuring the lengths of several dry-fibre specimens with 1 pulse/100mm, the dimensions of the typical entanglements produced by the splicer are displayed within Figure 1. Since intermingled regions interact with one another for specimens produced via multiple pulses, obtaining discrete entanglement dimensions is unsuitable for $> 1$ pulses/100mm specimens.

*Testing.* Tensile tests on the eight spliced sample variations and continuous tows were performed using an Instron 3369 Tensile Tester with a 10kN load cell. For each of the 9 specimen types, 75 specimens were tensile tested. To prevent stress concentrations and uneven load distributions at the specimen ends, two custom fixtures were machined. Aluminium cylinders were bolted to steel plates and a small clamping fixture was attached- see Figure 2(b). The custom fixtures were then locked onto the test machine by the crosshead grips. Specimens were first clamped to the upper fixture and wrapped twice around the upper aluminum cylinder. The lower part of the specimen was then wrapped and clamped to the lower fixture. Wrapping allowed for a gradual transfer of load to the specimen. For all configurations, the specimen gauge lengths was 250mm, and for spliced samples, the overlap region was positioned midway between the cylinders. Test rates were selected based upon specifications outlined in the Torayca TY-030B-01 test method [20]. A constant 30mm/min rate of vertical displacement was applied to the upper crosshead. Tests were stopped when the load dropped below 60% of the peak load.

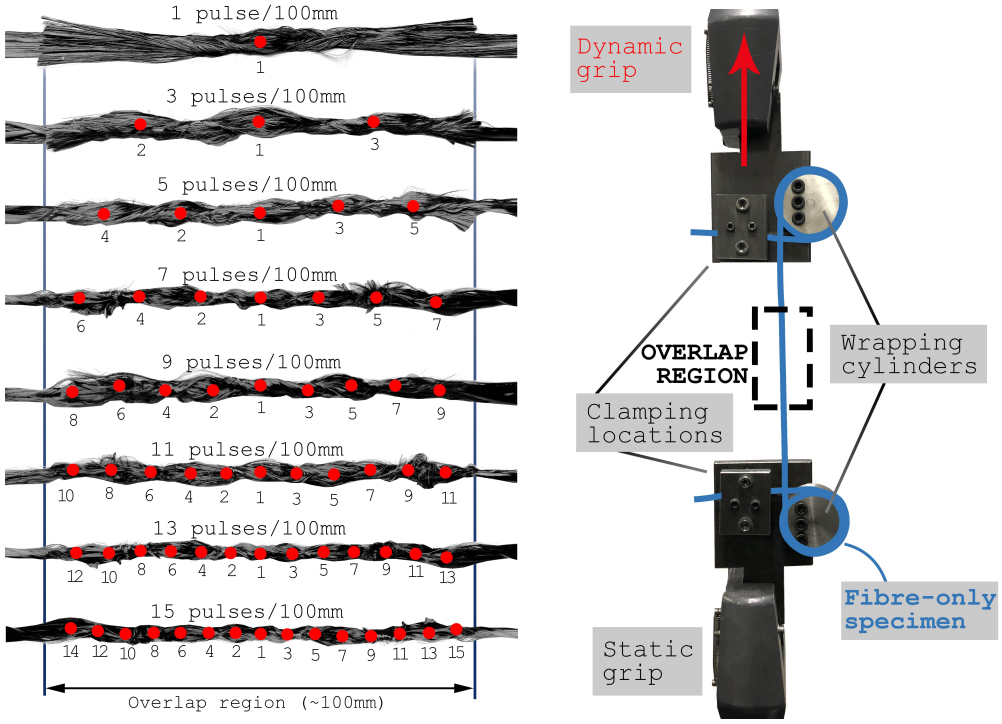


(a) Pulse Release Sequencing/Locations

(b) Annotated Dry-fibre Specimen Tensile Testing Diagram

Figure 2: Dry-fibre Specimen Manufacture and Testing

### *2.2. Composite Specimens*

*Materials.* As with the dry-fibre specimens, Toray T700SC-24K-50C carbon fibres were used [17]. Carbon fibre reinforced polymer (CFRP) composite plates were manufactured using epoxy powder (PE6405, density 1.22 g/cm$^3$) designed by Swiss CMT and produced by Freilacke [19]- details given in Table 1. Though this epoxy system melts between 45°C and 60°C, the polymer only starts to cure and crosslink above 150°C as it uses a heat-activated catalyst to initiate the cure (see Figure 3). This large temperature gap between the two phenomena allows for very thorough carbon fibre wetting and improved consolidation. The viscosity of the liquid resin drops with increased temperature, but crucially is not influenced by crosslinking until above 150°C. Maguire et al. showed that the dynamic viscosity of the liquid resin could be as low as 1.26 Pa·s before gelation occurs, whilst characterising epoxy powders for processing thick-section composite structures [21]. This powder system also enables a layer-by-layer manufacturing approach, allowing for good manufacturing control over the homogeneity and fibre volume fraction (FVF) of the composite. In the context of agglomerated and entangled fibres as expected from splicing, the powder allows both for better controlled manufacturing and lower

viscosities in comparison to standard liquid systems. Mechanical tests conducted on powder-based CFRP have also revealed promising results, including excellent fracture toughness, quasi-static tensile, fatigue and hygrothermally-aged properties [22, 23].

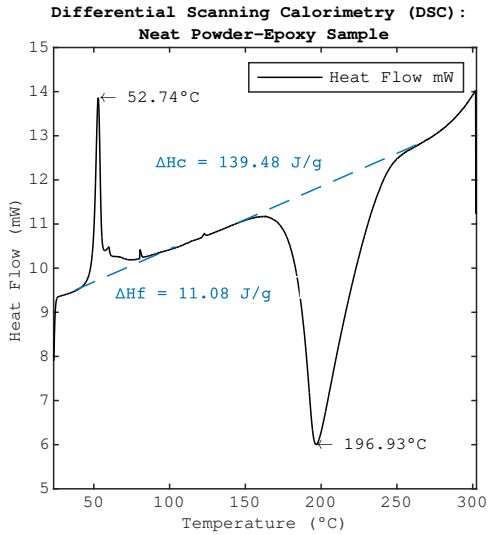


Figure 3: DSC Plot (Heat Flow/mW vs. Temperature/°C)
for Neat PE6405 Sample [21]

*Manufacture.* For all composite plates reinforced with pneumatically spliced material, tow-tow connections were formed by discharging nine pulses of air at equidistant locations along each 100mm overlap. A SPC value of 9 pulses/100mm was selected as calculated asymptotic regression functions for strength and linear stiffness showed significant diminishing returns beyond this value (see Section 3.1). The manufacture of composite panels embedded with pneumatically spliced tows poses unique challenges when compared to a conventional, manually laid unidirectional (UD) composite. The flat aspect ratio and consistent fibre direction seen in off-the-reel tows become more cylindrical and highly twisted after splicing. An obvious feature of spliced yarns is that the number of fibres along the overlapped region is doubled. By manufacturing a laminate with spliced overlaps positioned at its centre, adversely large FVFs would incur along the middle region whilst macrovoids will form elsewhere. To mitigate these issues, spliced overlaps must be positioned in staggered arrangements. Two approaches were developed in this study, such that at any location across the panel surface, the corresponding quantity of fibres through-the-thickness remains constant. These have been designated as spliced reinforcement configuration A (SRC-A) and B (SRC-B). The SRC-A configuration maximises the quantity of spliced overlaps within the panel; each reconstituted yarn is entirely made up of overlapped (and subsequently spliced) 200mm carbon fibre tow fragments. Yarns for SRC-B configuration plates instead contain

a single 100mm spliced overlap along their length, with the remaining 200mm of yarn length being non-entangled. Thus, SRC-B configurations contain only one spliced overlap per yarn, whilst SRC-A specimens contain three or four, depending on ply number. As illustrated in Figure 5, the yarns utilised for reinforcing SRC-A and SRC-B configurations are positioned in the unidirectional arrangements presented in subfigures (a) and (d-e). Along with spliced plates, UD and chopped strand mat (CSM) plates of the same material system were also tested for comparison. Although fibre orientation has significant bearing on the experimental outcomes, the randomly orientated CSM configuration represents a standardised arrangement for remanufactured/recycled composite panels. [24, 25] For this reason, it was deemed a valuable industrial benchmark for this preliminary investigation, since remanufacture/recycling is an important potential application for this technology. For each of the four layups (UD, SRC-A, SRC-B, CSM), both high and low processing pressure variants were considered; this allowed for pressure-material property relationships to be observed. Some details and specifications for each plate configuration are provided in Table 2.

Table 2: Composite Layup Specifications

| | Individual Yarn Details | | | | | |
|---|---|---|---|---|---|---|
| | Pressure (kPa) | Length (mm) | Orientation (degrees) | Tow Assembly | Tows per Ply | Config. Diagram |
| P5-UD | 500 | 300 | 0° | 300mm | 40 | Figure 5c |
| P5-SRC-B | 500 | 300 | 0° | 2×300 mm[b] | 30 | Figure 5e |
| P5-SRC-A | 500 | 300 | 0° | 5×200 mm[b] | 20 | Figure 5d |
| P5-CSM | 500 | 200 | R[a] | 200mm | 60 | Figure 5b |
| P2-UD | 200 | 300 | 0° | 300mm | 40 | Figure 5c |
| P2-SRC-B | 200 | 300 | 0° | 2×300 mm[b] | 30 | Figure 5e |
| P2-SRC-A | 200 | 300 | 0° | 5×200 mm[b] | 20 | Figure 5d |
| P2-CSM | 200 | 200 | R[a] | 200mm | 60 | Figure 5b |

[a] "R": Randomly Orientated.

[b] Tows are cut to size (200 or 300mm) and spliced into quasi-continuous yarns. These yarns are subsequently trimmed to 300mm lengths.

Prior to laying-up, a simple two-part rectangular mould was first machined from two 400mm×400mm×40mm 6082T aluminium blocks for plate manufacture, as specified in Figure 4. The geometry allowed for excess resin to leak from the mould during the pressurised melt-stage of the cure cycle. By using this mould, identical processing conditions could be applied to all composite layups in this work. The approach was selected as a means for producing consolidated specimens, despite the wettability and resin infusion characteristics of spliced fibrous material currently remaining unstudied. The low melt viscosity of the PE6405 powder promotes higher FVF when using a resin run-off based method. Prior to use, five layers of Loctite 770-NC Frekote release agent were applied to both mould tooling surfaces.

The layup process is presented visually, with diagrams for precise tow configurations for all plate types, in Figure 5. A manual hand-layup process was used to place six plies of tows directly on the

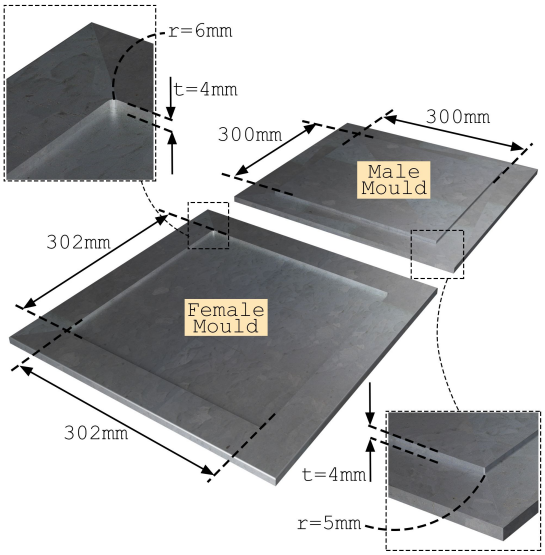


Figure 4: Mould Specifications

mould. For all plate types and pressures, the total PE6405 and T700SC-24K-50C tow weights were constant (listed in Table 3). For each plate, the epoxy mass was equally divided and set aside into seven containers. Similarly, the prepared yarns were split into six equal bundles (two bundles per splice stagger position). To maintain a consistent number of fibres through the panel thickness, the number of yarns per bundle (and thus yarns used in each ply) vary according to layup type- defined in Table 2. An initial layer of powder epoxy was dispersed over the mould tooling surface. Yarns from one bundle were then individually placed along the mould and subsequently sprinkled with one container of powder epoxy. This laying and sprinkling process was repeated until all the component materials had been used up. The male mould-part was then added and the assembled mould/layup was placed within a Radius Workstation 70 Tonne RTM/SQRTM press for curing. The curing cycle for all plates is displayed graphically in Figure 6. The dashed line indicates the time at which the pressure rises from 200kPa to 500kPa for the high pressure samples only (denoted P5); low pressure samples remain at 200kPa throughout the curing process (denoted P2). Notably, an extended melt-dwell time of 90 min (at 130°C) was selected to allow for maximum resin run-off to improve FVF. Once at 180°C, a constant (curing) temperature was held for 90 min. The ambient to melt temperature and melt to cure temperature ramp rates were set at 5°C/min and 3°C/min, respectively. Upon demoulding the composite plate, edges were trimmed and end tabs (Vector PCB GFRP) were bonded using VTFA400 adhesive film- supplied by SHD Composites Ltd. Specimens were then cut to size using a diamond bladed wet saw in accordance with geometry specified in ISO 527-5:2009 (Type A specimens)- shown in Figure 7(a).

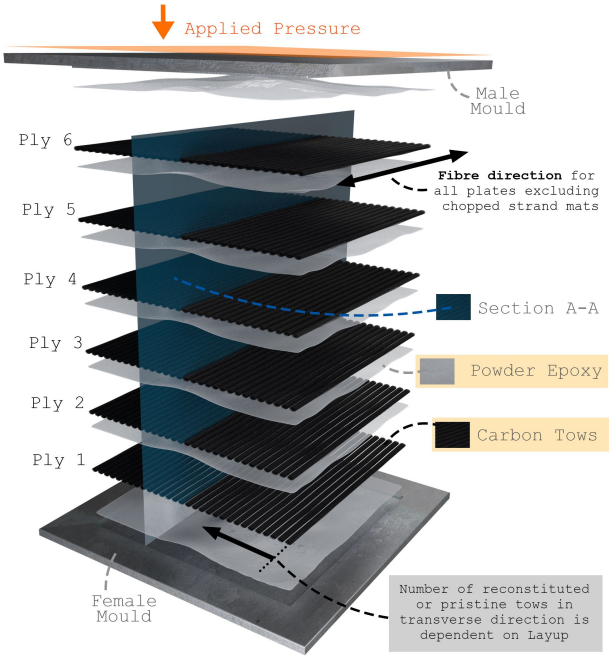


(a) Exploded Diagram of UD Composite Plate Assembly

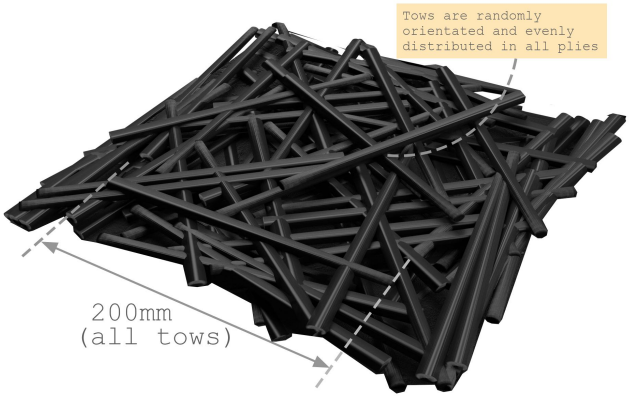


(b) Visualisation of Tow Orientation in CSM Ply

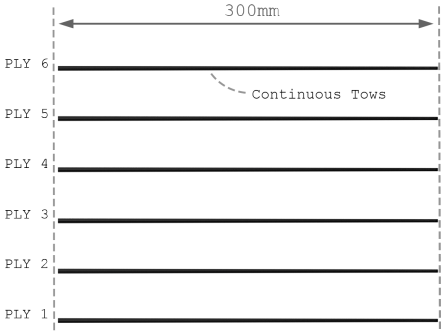


(c) Section A-A: UD Configuration

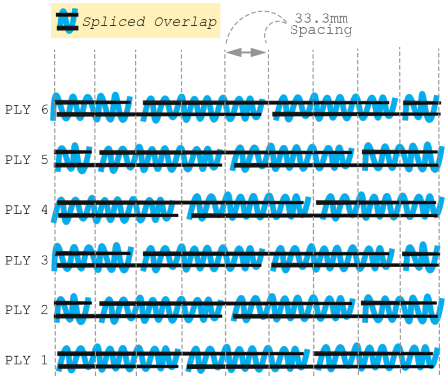


(d) Section A-A: SRC-A Configuration

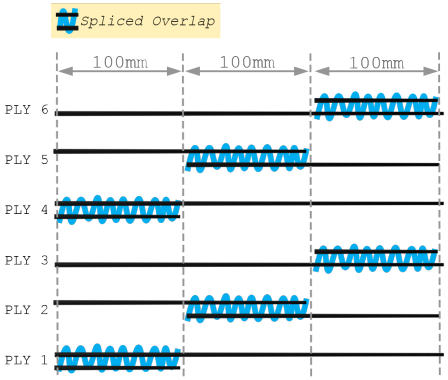


(e) Section A-A: SRC-B Configuration

Figure 5: Composite Panel Manufacture Details

Table 3: Manufacture Details

| | | |
|---|---|---|
| Material Quantities for Manufacture | Mass of Fibres (g) | 122 |
| | Mass of Epoxy (g) | 183 |
| | Number of Plies | 6 |
| Plate Details (from 6082T aluminium mould) | Length (mm) | 300.0 |
| | Width (mm) | 300.0 |
| | Thickness Range (mm) | $0 < t < 4.0$ |

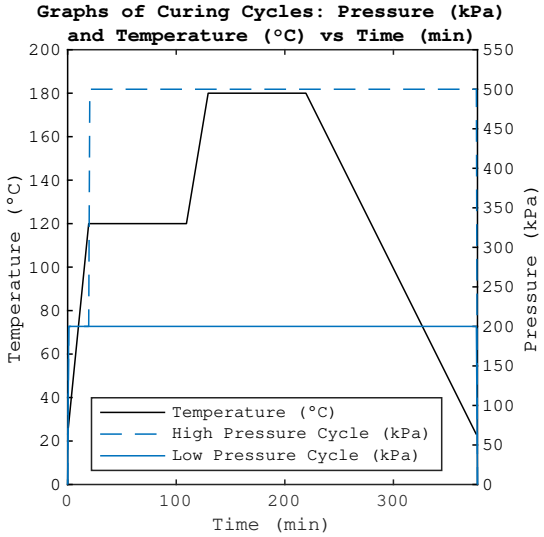


Figure 6: Curing Cycle Plot

*Testing.* Testing of composite specimens was based on ISO 527-5:2009 (supplemented where necessary with ISO 527-1:2019), using an MTS Criterion C45.305 electromechanical load frame fitted with a 300kN load cell and 647 hydraulic wedge grip. The test rate was controlled by crosshead extension and set to a constant rate of 2mm/min. Strain data was captured using an MTS AVX04 video extensometer package consisting of an Allied Vision Manta G-146 camera with Sill Optics Correctal T/0.2D lens and MTS AVX software package. The data sampling rate was consistent at $10.02 \pm 0.02$ measurements per second. Specimens were speckled with white spray paint to span the central third region. Specimen thickness and width were measured at three locations using a micrometer and vernier calipers, and averaged. In succession, the specimens were clamped in the load frame such that the crosshead grips evenly applied pressure to the entire tabbed region (136mm nominal initial grip separation) at a pressure of 550kPa. The loading axis was parallel to the long edge of the specimen. The extensometer system was set on a tripod and directed at the test machine to observe the specimen speckled region as shown in Figure 7(b). Tests were concluded at ultimate failure of the specimens, defined and detected automatically by the MTS Criterion as an instantaneous stress drop exceeding 90% of the preceding

value. Data for time, extension, load, principal strain, and specimen initial cross-sectional area was exported in a CSV file for each specimen for analysis using MATLAB R2019b.

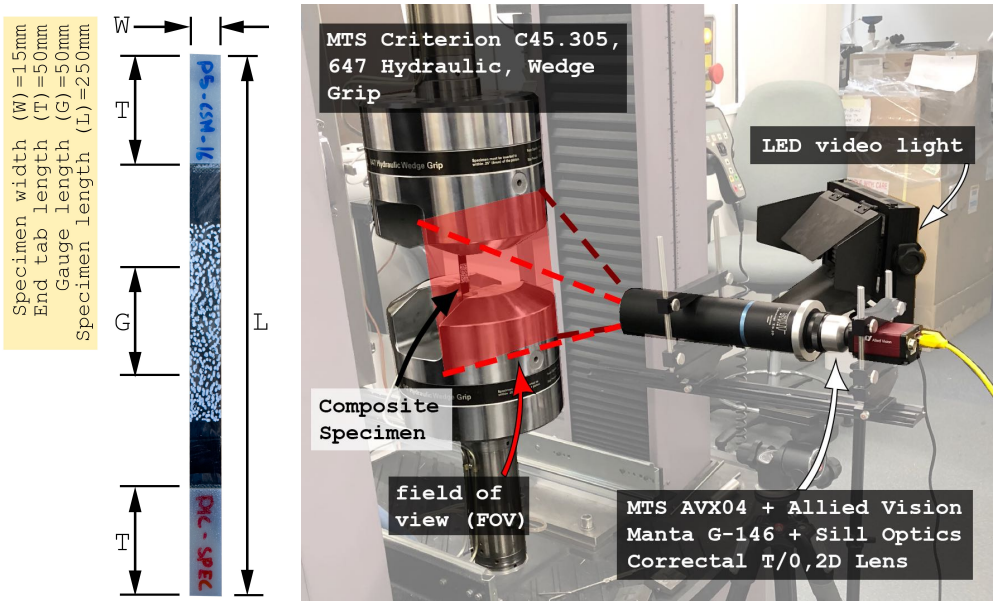


(a) Annotated Image of Test Specimen

(b) Labelled Photograph of Tensile Testing and Extensometer Setup for Composite Specimens

Figure 7: Composite Specimen Testing

*Characterisation.* Measurement of specimen density was completed using an Ohaus Adventurer AX324 Analytical Balance coupled with an Ohaus Density Determination Kit. For each test case, an extraction measuring approximately 100mm$^2$ was cut from five randomly selected tensile test specimens using a diamond bladed wet saw. Specimens were dried in a SciQuip 230HT oven at 50°C for 24h and further conditioned in a Prolan Pe70Cl50F40HV benchtop environmental chamber in accordance with ISO 291:2008. For each specimen, the dry mass and the mass while suspended in the working fluid was recorded. The working fluid used was tap water and the ambient temperature in the test environment was stable at 22°C. Matrix combustion was used for the measurement of FVF in accordance with ASTM D3171-15, Test Method I. The same five specimens per case as used in the density determination, were once again conditioned according to ISO 291:2008 in the same Prolan benchtop environmental chamber prior to the test. A Nabertherm L15/11 muffle furnace and Haldenwanger porcelain crucibles with lids were used to complete matrix combustion. An additional crucible containing traveller fibres verified that negligible fibre mass-loss occurred throughout the heating cycle.

*Imaging.* Scanning electron microscopy was performed to examine the orientation and distribution of fibres, using a Hitachi TM4000 low-vacuum microscope. Samples of size 15×15mm were extracted from remaining untested composite specimens and polished such that fibres were visible on the surface. A combination of back-scattered and secondary electrons was selected to provide both material and topological contrast. Images of resolution 2560×1920 were captured at 1.5k magnification using a 15kV accelerating voltage. A capture speed of 160 seconds was selected to reduce image grain. In all images, the width and height corresponds to the longitudinal and in-plane transverse directions of the specimen, respectively. Transient thermomechanical responses such as progressive damage mechanisms (for example, matrix cracking and fibre breakage) can be readily observed using infrared (IR) thermography techniques. A FLIR A655sc high-resolution infrared camera configured to a -40°C to 150°C temperature range was positioned roughly perpendicular to the sample (directly next to the extensometer system). Using an FOL25 lens, 640×480 resolution images were captured at a frame rate of 50 Hz. An object emissivity of 0.95, 20°C atmospheric temperature, 20°C reflected temperature and relative humidity of 50% were also inputted. FLIR ResearchIR Max software was used to process all image data. Bounds of $17.5°C > T > 50°C$ were used and a linear scale was selected to visualise temperature gradients.

## 3. Results

### *3.1. Dry-fibre Specimens*

*Tensile Testing.* Characteristic tensile responses for each specimen type are given in Figure 8. For each SPC, 75 specimens were tested and analysed. The compliance properties of the spliced specimens are compared to those of virgin tows by calculating the linear stiffness in N/mm. This metric was selected over Young's Modulus because the spliced overlap region has double the number of fibres present in a continuous tow. For a spliced configuration, "N/mm$^2$" would therefore have little physical meaning. Additionally, strain gauging and digital image correlation (DIC) are both unsuited to discrete dry-fibre bundles.

The linear stiffness of each specimen was obtained by calculating the gradient of its force-displacement plot. Given the lack of international test standard, a convergence study was performed using MATLAB 2019b software. For every specimen, stiffness values were calculated at every position along the length of the curve. Initially, a displacement interval of 0.05mm was used for all stiffness calculations. The maximum obtained stiffness value from each sample was then recorded (for each individual sample). For each SPC, an average of these "maximum" values was then calculated. The same procedure was then repeated using displacement intervals ranging from 0.05mm to 5.00mm (in 0.05mm increments). To undertake these calculations, a series of nested loops were implemented within MATLAB scripts

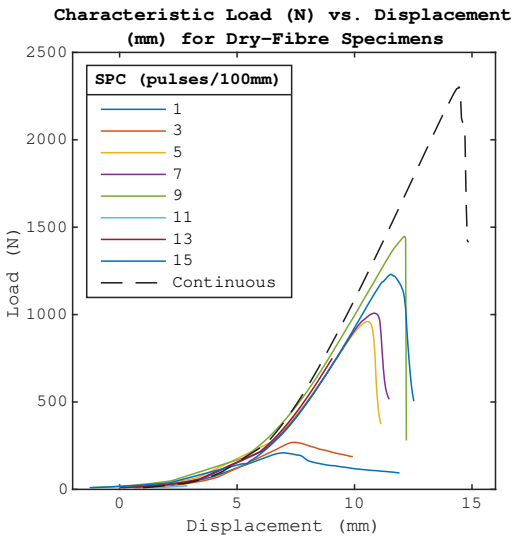


Figure 8: Load (N) vs. Displacement (mm) Plot
Dry-fibre Specimens

to automate the process. In plotting the results from this analysis (Figure 9), the calculated average stiffness marginally decreases as the displacement interval size increases. Stiffness data was evaluated over displacement intervals spanning 1mm, which is presented in Table 4 and Figure 9. Percentage recoveries relative to continuous fibre specimen performances are also reported, and are denoted by P-REC.

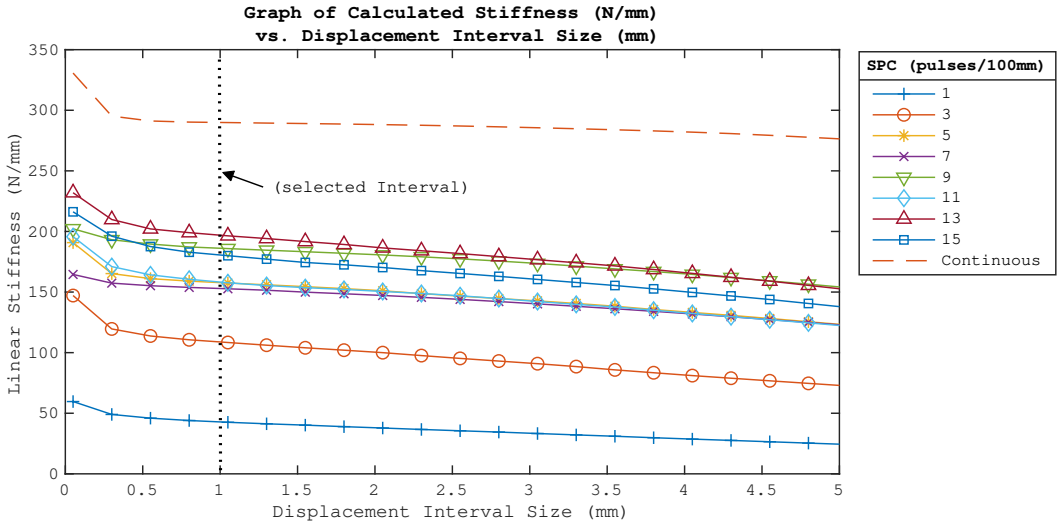


Figure 9: Graph of Linear Stiffness (N/mm) vs. Crosshead
Interval Size (mm) for Dry-fibre Specimens

Table 4: Tensile Testing Results for Dry-fibre Specimens

| | Linear Stiffness (N/mm) | | | | Failure Loads (N) | | | |
|---|---|---|---|---|---|---|---|---|
| SPC (pulses/100mm) | Mean | SD | CoV (%) | P-REC (%) | Mean | SD | CoV (%) | P-REC (%) |
| (Cont.) | 294.4 | 17.9 | 6.2 | - | 2230.0 | 129.9 | 5.8 | - |
| 15 | 183.5 | 47.4 | 25.8 | 62.3 | 876.3 | 258.6 | 29.5 | 39.3 |
| 13 | 199.5 | 47.4 | 23.8 | 67.8 | 957.0 | 281.0 | 29.4 | 42.9 |
| 11 | 161.2 | 47.7 | 30.6 | 54.8 | 805.9 | 277.2 | 34.4 | 36.1 |
| 9 | 187.9 | 46.7 | 26.2 | 63.8 | 1026.8 | 388.5 | 37.8 | 46.0 |
| 7 | 154.1 | 76.5 | 49.7 | 52.3 | 803.6 | 472.7 | 58.8 | 36.0 |
| 5 | 159.4 | 54.3 | 34.4 | 54.1 | 785.2 | 365.5 | 46.6 | 35.2 |
| 3 | 111.1 | 45.7 | 41.2 | 37.7 | 428.2 | 214.8 | 50.2 | 19.2 |
| 1 | 44.3 | 29.0 | 63.6 | 15.0 | 145.7 | 108.5 | 74.5 | 6.5 |

*Number of specimens tested per SPC group: 75

Failure loads were evaluated using a similar approach to linear stiffness. Again, a series of nested loops were used to evaluate the maximum recorded load for every sample of each SPC. The mean, standard deviation and coefficient of variance values (along with percentage recovery relative to continuous fibre specimens, P-REC) of the specimen maxima are provided in Table 4. Additionally, plots of mean failure load and linear stiffness (implementing standard deviation, SD bars) versus SPC are provided in Figure 10. For both Figures 10(a) and (b), a least squares optimisation algorithm was utilised to calculate asymptotic regression fit-lines of the form provided in Equation 1, where $\alpha$ is the asymptote of the function $f(x)$, $\beta$ is the origin location, $\gamma$ defines the rate of convergence and $x$ denotes the $SPC$.

$$f(x) = \alpha - (\alpha - \beta)e^{-\gamma x} \tag{1}$$

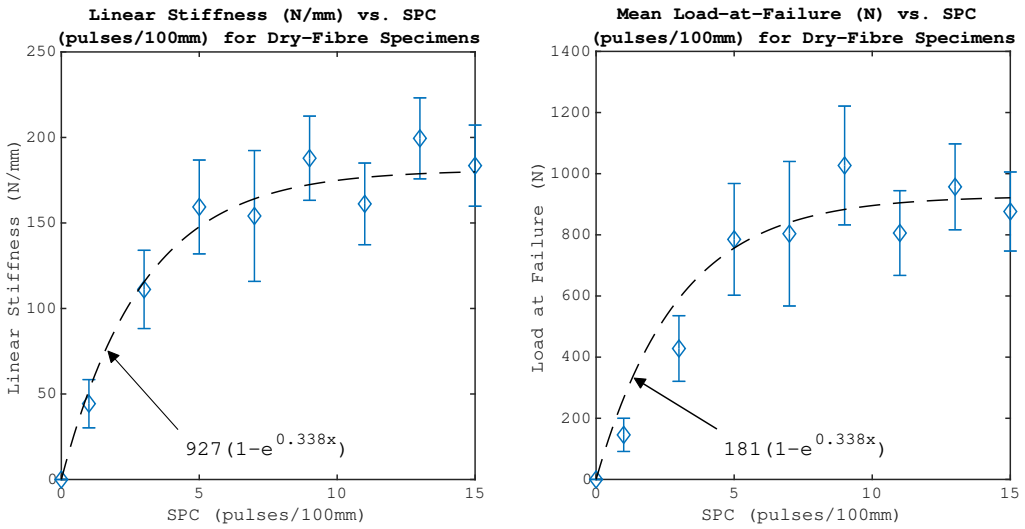


(a) Linear Stiffness

(b) Failure Load

Figure 10: Dry-fibre Specimen Tensile Performance
. SPC (Mean Values With Standard Deviation, SD bars)

### *3.2. Composite Specimens*

*Tensile Testing.* Ten composite specimens per configuration were tested in accordance with ISO 527-1:2019- representative stress-strain plots for each configuration are presented in Figure 11. Regression analysis was completed to obtain the measurements for Young's Modulus; the results of which are contained in Figure 12(a) and Table 5. Similarly, the ultimate tensile strength (UTS) results are also provided in Figure 12(b) and Table 5. The mean moduli and ultimate strengths achieved by each configuration are further reported as percentages of the equivalent-pressure UD configuration results (P-REC) in Table 5.

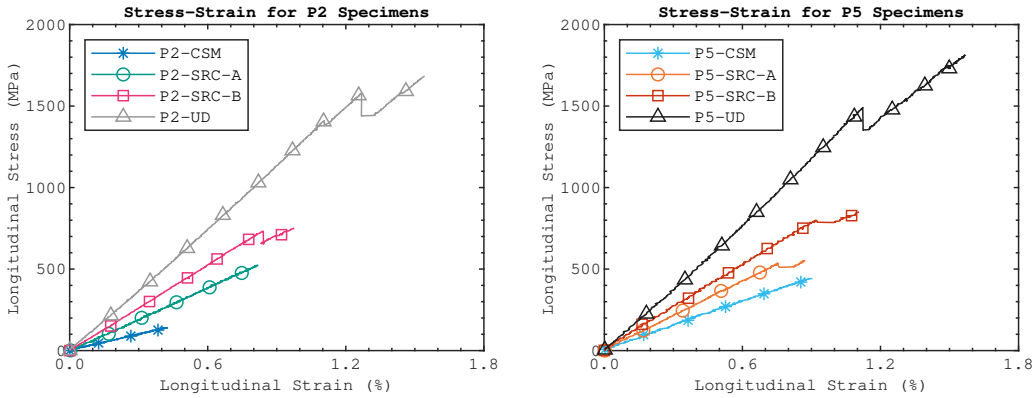


(a) P2, Stress vs. Strain

(b) P5, Stress vs. Strain

Figure 11: Tensile Test Results of
Representative Composite Specimens

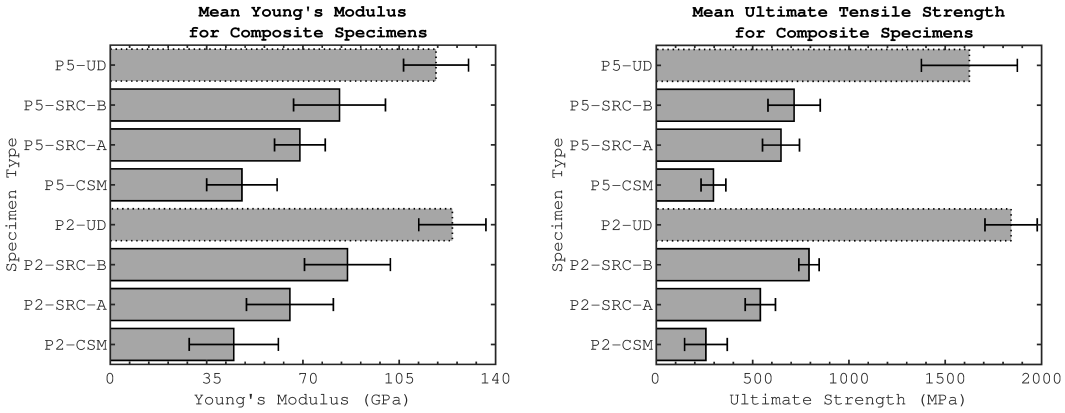


(a) Young's Modulus

(b) Ultimate Strength

Figure 12: Composite Specimen Tensile Testing
Results (Mean Values with Standard Deviation, SD Bars)

Table 5: Tensile Testing Results for Composite Specimens

| | Young's Modulus, $E_1$ (GPa) | | | | Ultimate Stress, $\sigma_b$ (MPa) | | | |
|---|---|---|---|---|---|---|---|---|
| | Mean | SD | CoV (%) | P-REC (%) | Mean | SD | CoV (%) | P-REC (%) |
| P5-UD | 118.4 | 11.8 | 10.0 | - | 1625.3 | 249.0 | 15.3 | - |
| P5-SRC-B | 83.3 | 16.7 | 20.2 | 70.4 | 715.4 | 135.5 | 18.9 | 44.0 |
| P5-SRC-A | 68.9 | 9.2 | 13.3 | 58.2 | 647.2 | 96.0 | 14.8 | 39.8 |
| P5-CSM | 47.8 | 12.8 | 26.8 | 40.4 | 296.5 | 64.3 | 21.7 | 18.2 |
| P2-UD | 124.3 | 12.2 | 9.8 | - | 1842 | 135.5 | 7.4 | - |
| P2-SRC-B | 86.2 | 15.6 | 18.1 | 69.3 | 792.7 | 52.7 | 6.6 | 43.0 |
| P2-SRC-A | 65.3 | 15.8 | 24.2 | 52.5 | 540.1 | 78.4 | 14.5 | 29.3 |
| P2-CSM | 44.9 | 16.2 | 36.2 | 36.1 | 257.6 | 110.9 | 43.0 | 14.0 |

*Number of specimens tested per configuration: 10

*IR Thermography and SEM.* Characteristic thermal responses for each P5 composite sample type at ultimate failure (as defined previously) are presented in Figure 13. Separate images have been compiled into an individual figure using Adobe Photoshop CC 2019. For all cases, colour, contrast and brightness remain that of the unaltered-raw images. Imaging of P2 composite specimens is indistinguishable from P5 configurations and thus, not included. Scanning Electron Microscope (SEM) images in Figure 14 show the fibre distribution for all P5 composite configurations. Images have been annotated to show global and local fibre directions, and entangled regions.

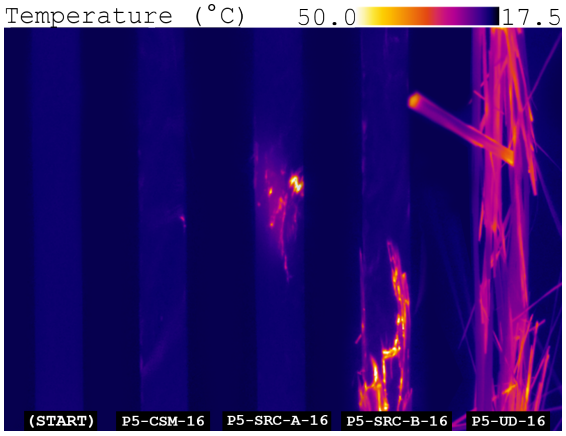


Figure 13: IR Thermography Imaging of P5 Composite Specimens at Ultimate Failure

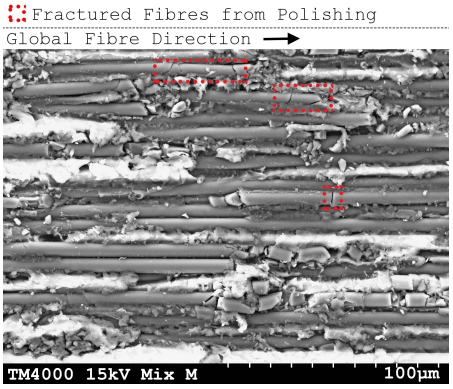


(a) P5-UD (non-spliced location)

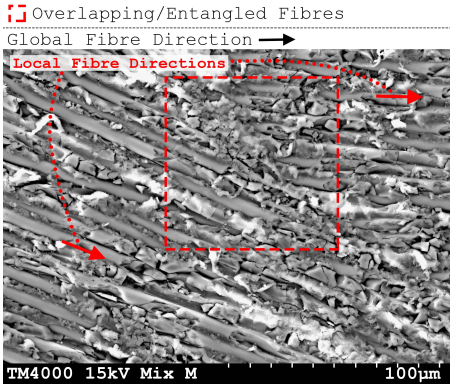


(b) P5-SRC-B (spliced location)

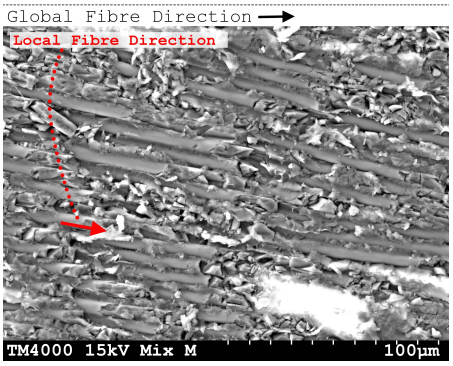


(c) P5-SRC-B (non-spliced location)

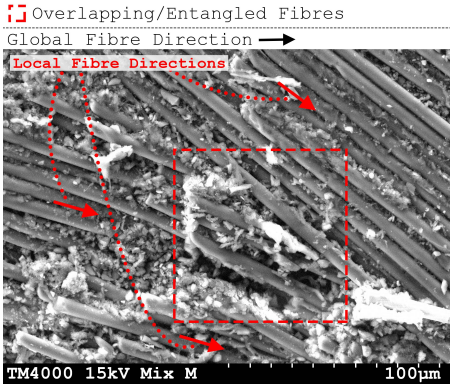


(d) P5-SRC-A (spliced location)

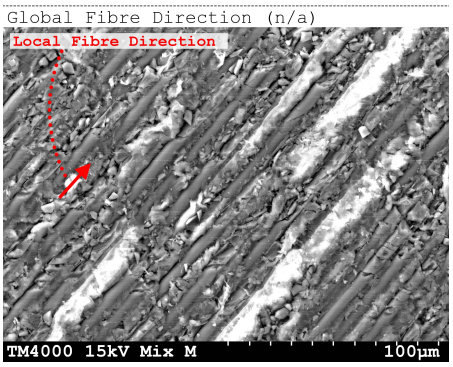


(e) P5-CSM (non-spliced location)

Figure 14: Annotated SEM images
of P5 Composite Specimen Surfaces

*Density and FVF.* Density of composite specimens ($\rho$) was obtained using Equation 2, where: $A$ is the dry mass, $B$ is the submerged mass, $\rho_O$ is the density of the tap water (997.56 kg/m$^3$) and $\rho_L$ is the density of air (1.2 kg/m$^3$).

$$\rho = \frac{A}{A-B}(\rho_O - \rho_L) + \rho_L \tag{2}$$

FVFs of composite specimens were obtained in accordance with the standard test method ASTM D3171-15. Equation 3 (transcribed) was used to calculate FVF, where: $M_i$ is the initial mass of specimen before combustion, $M_f$ is the final mass of specimen after combustion, $\rho_r$ is the density of the fibre and $\rho_m$ is the density of the cured epoxy. The densities, FVF and thicknesses of the five specimens per configuration were averaged and are presented in Table 6 and Figure 15.

$$FVF(\%) = \frac{M_f}{M_i} \times \frac{\rho}{\rho_r} \times 100 \tag{3}$$

Table 6: Composite Plate Characterisation Results:
Density, Fibre Volume Fraction and Thickness

| | $\rho$ (kg/m$^3$) | | | $FVF$ (%) | | | Thickness (mm) | | |
|---|---|---|---|---|---|---|---|---|---|
| | Mean | SD | CoV (%) | Mean | SD | CoV | Mean | SD | CoV (%) |
| P5-UD | 1.55 | 0.00 | 0.29 | 58.1 | 1.0 | 1.7 | 1.25 | 0.11 | 9.05 |
| P5-SRC-B | 1.52 | 0.01 | 0.61 | 51.7 | 2.5 | 4.9 | 1.56 | 0.07 | 4.36 |
| P5-SRC-A | 1.50 | 0.02 | 1.57 | 46.0 | 1.8 | 3.9 | 1.76 | 0.15 | 8.31 |
| P5-CSM | 1.50 | 0.04 | 2.72 | 40.3 | 1.5 | 3.8 | 1.93 | 0.16 | 8.12 |
| P2-UD | 1.50 | 0.02 | 1.15 | 51.3 | 3.2 | 6.3 | 1.37 | 0.03 | 1.90 |
| P2-SRC-B | 1.44 | 0.02 | 1.47 | 45.0 | 3.6 | 8.1 | 1.86 | 0.03 | 1.40 |
| P2-SRC-A | 1.39 | 0.04 | 3.06 | 39.8 | 2.5 | 6.2 | 2.17 | 0.10 | 4.60 |
| P2-CSM | 1.41 | 0.01 | 0.94 | 37.6 | 3.5 | 8.5 | 1.83 | 0.12 | 6.49 |

*Number of specimens tested per configuration: 5

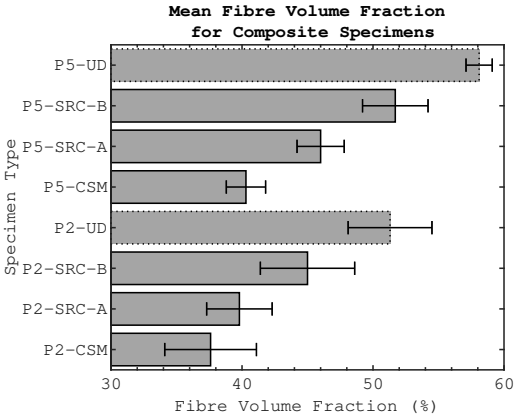


Figure 15: Fibre Volume Fraction Results for Composite Specimens (Mean Values with Standard Deviation, SD Bars)

## 4. Discussion

*Dry-fibre Specimens.* Given that spliced connections use no external adhesion or mechanical fasteners and rely purely on entanglement and friction, the load bearing capacity values of spliced dry-fibre specimens show outstanding potential for the future of pneumatic splicing for carbon fibre reinforcement. It is evident that splices undergo a slack removal process, effectively acting like constrictor knots, indicated by gradual stiffness increase in Figure 8. Overall, clear statistical trends are observed in Figure 10, where increasing SPC results in gains in strength and stiffness. Notably, particularly beyond SPC values of approximately 9 pulses/100mm, the gradients of these curves gradually transition towards zero, with linear stiffness and failure loads asymptotically approaching 181N/mm and 927N respectively. For these reasons, 9 pulses/100mm was chosen as the SPC for the composites reinforcement study. Specimens with SPC of 9 pulses/100mm withstood 1.027kN on average. In percentage terms, this equates to 46.0% of the mean failure load of the continuous carbon tows. Comparing Coefficient of Variance (CoV) for failure load, 9 pulses/100mm specimens had a wider spread of data, at 37.8% versus 5.8% for continuous specimens. Notably, increasing SPC has been shown to predominantly decrease the spread of data as denoted by CoV values in Table 4. Upon evaluation of standard z-scores, the minimum recorded 164.86N failure load for 9 pulses/100mm specimens would equate to -2.22 standard deviations from the mean. Assuming the distribution is Gaussian, this is equivalent to a 1.4% probability of occurrence. As with load bearing capacity results, stiffness results are exceptionally promising with 9 pulses/100mm specimens maintaining 63.8% of the mean stiffness of the continuous tows. Overall, these results prove that non-embedded pneumatically spliced carbon fibre tows are capable of carrying high loads with minimal straining (after slack removal). With further research, it is speculated that quasi-continuous yarns, remanufactured by splicing waste fibres, could provide a novel material for weaving, braiding, non-crimp fabrics, or in 3D printing applications.

*Composite Specimens.* The mean UTS bars in Figure 12 exhibit a clear performance hierarchy for the four layup variations (UD>SRC-B>SRC-A>CSM); this is apparent for both P2 and P5 manufacturing pressures. Where P5-UD and P2-UD results act as a benchmark, the overall performance of other specimens are compared in terms of recovered percentages (shown as P-REC in Table 5). For instance, the tensile strength of P2-SRC-A and P2-SRC-B specimens are equivalent to 29.3% and 43.0% of the corresponding P2-UD value. At the higher (500 kPa) manufacturing pressure, the tensile strength recovery of P5-SRC-A and P5-SRC-B specimens are 39.8% and 44.0% of the P5-UD value. Examining Figure 12, higher curing pressures resulted in marginally increased tensile strength for SRC-A and CSM specimens, and a small drop-off in tensile strength for UD and SRC-B specimens. Although CSM configurations have fibre orientation distribution factors of approximately 0.375 (as compared with 1.0 for UD) [26], they provide a useful datum for gauging the performance of spliced configurations

against more conventional remanufacturing approaches. P2-CSM and P5-CSM specimens recorded mean tensile strength values equivalent to recovery of 14.0% and 18.2% of P2-UD and P5-UD specimens, respectively.

Examining the Young's Moduli values in Figure 12, an identical performance hierarchy is observed for both manufacturing pressure variants (UD>SRC-B>SRC-A>CSM). For this metric, P2-SRC-A and P2-SRC-B mean values are equivalent to 52.5% and 69.3% of the P2-UD Modulus. As with tensile strength, increasing the curing pressure has marginal impact on stiffness, where P5-SRC-A and P5-SRC-B means are equivalent to 58.2% and 70.4% of the P5-UD value. In comparing the stiffness of spliced and CSM configurations, spliced specimens exhibit higher performance in all layup configurations, primarily due to global fibre alignment. Considering Figure 15, higher curing pressure consistently yields increased FVF, although this does not necessarily translate to increased Young's Modulus or UTS values. It is observed that increased pressure improves the mechanical performances of CSM and SRC-A specimens, but a minor performance reduction is seen in SRC-B and UD specimens. The observed increase in mechanical performance of P5-SRC-A and P5-CSM specimens is attributed to improved consolidation. The reduced fibre volume fraction in SRC-A specimens (relative to their SRC-B counterparts) is a result of additional fibre entanglement and overlapping. It is postulated that increasing the number of twisted and overlapped fibres reduces the compressibility of material during curing. The reduced thickness of SRC-B plates (mean thicknesses of 1.56mm and 1.86mm for 500kPa and 200kPa pressures respectively) compared to the SRC-A plates (means of 1.76mm and 2.17mm respectively) also support this postulation. The run-off manufacturing procedure has resulted in optically well consolidated panels which exhibit consistent densities, further suggesting that thickness reductions and FVF increases are a result of the increased flattening of reinforcing fibres (during the melt stage) whilst under compression. It is well documented that stiffness and quasi-static strength are proportional to FVF for composites. [27, 28] In other studies which consider carbon-epoxy systems, failure mechanisms have been observed to shift from matrix cracking and fibre-matrix debonding at low FVFs, to fibre pull out and bridging with increased fibre content. [29] For reasons such as these, reductions in mechanical properties can be anticipated for SRC-A configurations, although processing condition refinements could potentially alleviate these effects. Since resin is permitted to run-off from the mould cavity, fibre bundles are less likely to slide and displace with decreased flow. It is speculated that UD and SRC-B specimens are more sensitive to the effects of fibre misalignment (from resin run-off) than to gains in consolidation from higher processing pressures. Some additional validation is provided in the work of Mamalis et al [30], where an identical material system was used for evaluating the effects of fibre pre-tensioning. The mean UTS and Young's Modulus of P2-UD specimens was equivalent to 92.7% and 107.9% of the results reported by Mamalis et al, respectively.

Upon inspection of Figure 11, stress-strain distributions are elastically linear prior to damage

initiation in all cases. In UD specimens, material damage is denoted by instantaneous stress release followed by further linear straining and subsequently, brittle failure. Viewing the SEM image in Figure 14(a), individual fibre orientations are generally consistent with the global orientation of tows in UD specimens. Furthermore, from examining IR results in Figure 13, the UD specimens undergo explosive failure and produce significantly more heat. Considering failure loads, it is reasonable to assume that UD specimens undergo sudden fibre failure. Spliced specimens present more variance in their damage mechanisms, exhibiting both brittle and gradual damage propagation. Figure 14(b) and (d) show the spliced regions with entangled, overlapping fibre bundles and random local alignment. In viewing the thermal distribution of spliced specimens in Figure 13, the P5-SRC-A-16 and P5-SRC-B-16 specimens undergo a more localised failure, attributed to a combination of fibre breaks and matrix cracking. It was observed that CSM specimens produced minimal heat upon failure since they undergo failure as a result of debonding of off-axis fibres and consequent matrix cracking.

The composite results obtained provide foundation for further work; spliced specimens achieve high stiffness values (mean P5-SRC-A Young's Modulus of 68.9GPa) and respectable failure stresses (mean P5-SRC-A tensile strength of 647.2MPa). The design of a mould which induces yarn pretension, whilst also simultaneously applying through-thickness pressure during curing, may provide a means of maximising fibre to fibre load transfer through contact friction. Additionally, an optimised mould could allow for improved control of tow alignment and fibre volume fraction. Even with improvements in spliced plate manufacturing techniques, the splicing process requires individual fibres to be twisted and entangled together. For this reason, a certain degree of local fibre non-alignment will always be expected (particularly at or near the spliced region). Embedding splices within twills or other woven fabrics is expected to be even more promising, since overlapping tows could provide lateral constraint to the splice.

## 5. Conclusions

A preliminary investigation on a novel method of embedding spliced carbon fibre tows as reinforcement within composite panels has been undertaken. Outcomes of the present work establish the viability of utilising pneumatic splicing, of discontinuous carbon fibre tows, as a technique for remanufacture of waste composite materials. Firstly, an in-depth analysis of the tensile performance of spliced carbon fibre tows was considered. Results indicate that spliced connections are capable of recovering a significant proportion of the strength and stiffness of continuous carbon fibre tows. For instance, the best performing dry-fibre configuration maintained 46.0% of the mean continuous tow failure load. Excellent stiffness retention has also been observed, with specimens formed by discharging 9 pulses/100mm overlap maintaining 63.8% of the continuous tows' stiffness on average.

Carbon fibre tows joined with 9 pulses/100mm per overlap were then embedded as reinforcements in composite panels at different manufacturing pressures. Two spliced fibre assembly configurations were tested, which both exhibited impressive performance when compared to unidirectional specimens manufactured with continuous fibre reinforcement, under identical cure processing conditions. Specimens reinforced with a combination spliced material and continuous fibres, recovered 69-70% and 43-44% of the Young's Modulus and ultimate tensile strength, respectively. Similarly, specimens reinforced entirely with spliced material recovered 53-58% and 29-39% of the same respective metrics. Randomly orientated (in-plane) mats were also manufactured under identical processing conditions, and characterised to provide reference against more conventional remanufactured plate configurations. In all cases, the spliced configurations showed greater recovery of mechanical properties, relative to the unidirectional configurations, albeit partially due to higher degrees of global fibre alignment and fibre volume fractions.

The encouraging results of this work demonstrate that splicing of carbon fibre tows should undergo further research. Upon completion of a robust design of experiments, it is anticipated that the mechanical properties of spliced carbon fibre tows will be further demonstrated. With respect to embedded-splices, potential avenues to investigate include improved mould design, 3D-print filament reinforcement and weaving of spliced tows; all of which could contribute towards a novel, high value composite remanufacturing solution.

## 6. Acknowledgements

The support of MacTaggart, Scott & Co. Ltd. and Engineering and Physical Sciences Research Council (EPSRC) under the National Productivity Investment Fund (NPIF) are gratefully acknowledged. The authors would like to thank: Mr. Lee Baines and Dr. Terry McGrail for their guidance and feedback; Prof. Luke Bisby and Mr. Michal Krajcovic for their providing access to, and guidance for, the FLIR infrared camera. The invaluable advice from technical staff member, Mr. Edward Monteith has also been greatly appreciated throughout this work.

## References

[1] Advanced Composites Manufacturers Association (ACMA), "Storage Tanks: Built to Last"- The Official Magazine of the Advanced Composites Manufacturers Association, CompositesManufacturing (January/February) (2020).

[2] S. Halliwell, Frps—the environmental agenda, Advances in structural engineering 13 (5) (2010) 783–791.

[3] P. Davies, Y. D. Rajapakse, Durability of composites in a marine environment, Vol. 208, Springer, 2014.

[4] A. Subic, A. Mouritz, O. Troynikov, Sustainable design and environmental impact of materials in sports products, Sports Technology 2 (3-4) (2009) 67–79. doi:10.1002/jst.117.

[5] J. Zhang, V. S. Chevali, H. Wang, C. H. Wang, Current status of carbon fibre and carbon fibre composites recycling, Composites Part B: Engineering 193 (December 2019) (2020) 108053. doi:10.1016/j.compositesb.2020.108053.
URL https://doi.org/10.1016/j.compositesb.2020.108053

[6] Y. Liu, L. Meng, Y. Huang, J. Du, Recycling of carbon/epoxy composites, Journal of Applied Polymer Science 94 (5) (2004) 1912–1916. doi:10.1002/app.20990.

[7] K. Iwnicki, Process and apparatus for Joining Yarns or Tows (GB956992A) (1964).
URL https://patents.google.com/patent/GB956992A/en

[8] B. Satapathy, J. Bijwe, Performance of friction materials based on variation in nature of organic fibres: Part i. fade and recovery behaviour, Wear 257 (5-6) (2004) 573–584.

[9] R. C. D. Kaushik, P. K. Hari, I. C. Sharma, Mechanism of the Splice, Textile Research Journal 58 (5) (1988) 263–268.

[10] C. J. Webb, Investigation and Modelling of the Yarn Splicing Process, Ph.D. thesis, The University of Glamorgan (2008).

[11] G. Basal, The structure and properties of vortex and compact spun yarns, North Carolina State University, 2003.

[12] A. Primentas, C. Iype, The configuration of textile fibers in staple yarns, J Text Apparel Technol Manag 1 (2001) 1–8.

[13] S. Lewandowski, R. Drobina, Strength and geometric sizes of pneumatically spliced combed wool ring spun yarns, Fibres and Textiles in Eastern Europe 12 (2) (2004) 31–37.

[14] C. J. Webb, G. T. Waters, A. J. Thomas, G. P. Liu, C. Thomas, The use of the Taguchi design of experiment method in optimizing splicing conditions for a Nylon 66 yarn, Journal of the Textile Institute 98 (4) (2007) 327–336. doi:10.1080/00405000701489255.

[15] C. J. Webb, G. T. Waters, G. P. Liu, C. Thomas, The Influence of Yarn Count on the Splicing of Simple Continuous Filament Synthetic Yarns, Textile Research Journal 79 (3) (2009) 195–204. doi:10.1177/0040517508094396.

[16] C. J. Webb, G. T. Waters, A. J. Thomas, G. P. Liu, E. J. Thomas, Optimising splicing parameters for splice aesthetics for a continuous filament synthetic yarn, Journal of the Textile Institute 100 (2) (2009) 141–151. doi:10.1080/00405000701660087.

[17] Torayca, Explanation of Product Code 2–1.
URL http://www.toraycfa.com/pdfs/ExplanationofProductCode.pdf

[18] TorayCA, T700S Technical Data Sheet (2005) 2doi:CFA-005.
URL http://www.toraycfa.com/pdfs/T700SDataSheet.pdf

[19] D. Mamalis, J. J. Murray, J. McClements, D. Tsikritsis, V. Koutsos, E. D. McCarthy, C. M. Ó Brádaigh, Novel carbon-fibre powder-epoxy composites: Interface phenomena and interlaminar fracture behaviour, Composites Part B: Engineering 174 (June) (2019). doi:10.1016/j.compositesb.2019.107012.

[20] Torayca, TY-030B-01 (Test Method), Tech. rep., Toray Carbon Fibres America, Inc., Santa Ana, CA.
URL www.toray.com

[21] J. M. Maguire, K. Nayak, C. M. Ó Brádaigh, Characterisation of epoxy powders for processing thick-section composite structures, Materials and Design 139 (2018) 112–121. doi:10.1016/j.matdes.2017.10.068.
URL https://doi.org/10.1016/j.matdes.2017.10.068

[22] C. Robert, T. Pecur, J. M. Maguire, A. D. Lafferty, E. D. McCarthy, C. M. Brádaigh, A novel powder-epoxy towpregging line for wind and tidal turbine blades, Composites Part B: Engineering 203 (October) (2020). doi:10.1016/j.compositesb.2020.108443.

[23] C. Floreani, C. Robert, P. Alam, P. Davies, C. M. Ó Brádaigh, Characterization of mode I interlaminar properties of novel composites for tidal turbine blades, in: EWTEC 2019 – 13th European Wave and Tidal Energy Conference, no. September, Naples, Italy, 2019.
URL https://www.researchgate.net/publication/334163936

[24] S. Pompidou, M. Prinçaud, N. Perry, D. Leray, Recycling of carbon fiber: Identification of bases for a synergy between recyclers and designers, in: Engineering Systems Design and Analysis, Vol. 44861, American Society of Mechanical Engineers, 2012, pp. 551–560.

[25] P. R. Barnett, B. M. Hulett, D. Penumadu, Crashworthiness of recycled carbon fiber composites, Composite Structures 272 (2021) 114232.

[26] L. Harper, T. Turner, N. Warrior, J. Dahl, C. Rudd, Characterisation of random carbon fibre composites from a directed fibre preforming process: Analysis of microstructural parameters, Composites Part A: Applied Science and Manufacturing 37 (11) (2006) 2136–2147. doi:https://doi.org/10.1016/j.compositesa.2005.11.014.
URL https://www.sciencedirect.com/science/article/pii/S1359835X05004136

[27] M. Karahan, The effect of fibre volume fraction on damage initiation and propagation of woven carbon-epoxy multi-layer composites, Textile Research Journal 82 (1) (2012) 45–61.

[28] J. Brunbauer, H. Stadler, G. Pinter, Mechanical properties, fatigue damage and microstructure of carbon/epoxy laminates depending on fibre volume content, International Journal of Fatigue 70 (2015) 85–92.

[29] K. Mini, M. Lakshmanan, L. Mathew, M. Mukundan, Effect of fibre volume fraction on fatigue behaviour of glass fibre reinforced composite, Fatigue & Fracture of Engineering Materials & Structures 35 (12) (2012) 1160–1166.

[30] D. Mamalis, T. Flanagan, C. M. Ó Brádaigh, Effect of fibre straightness and sizing in carbon fibre reinforced powder epoxy composites, Composites Part A: Applied Science and Manufacturing 110 (2018) 93–105.